ROYAL SOCIETY OF CHEMISTRY

PAPER

Check for updates

Simultaneous digital and analog resistive switching in a polymorphic copper sulfide thin film-based memristor

Rajesh Deb, [ID] [a] Farhana Yasmin, [ID] [a] Yamineekanta Mishra, [ID] [a] Zarina Azmi, [ID] [a] Dibakar Sahoo [ID] [b] and Saumya R. Mohapatra [ID] *[a]

Analog resistive switching characteristics are recognized as more suitable for neuromorphic computing due to their gradual change in resistance states, energy efficiency, and inherent parallel processing capabilities. The analog switching behaviors are primarily influenced by the switching medium, particularly materials exhibiting mixed ionic and electronic conductivity. In this study, a copper sulfide-based memristive device was fabricated using the chemical bath deposition (CBD), with copper as the active electrode. The CBD-grown copper sulfide is polymorphic in form ($Cu_{2-x}S$) as evident from X-ray photoelectron spectroscopy (XPS) and energy dispersive spectroscopy (EDS) studies. The carrier concentration calculated using Mott–Schottky plots is of the order of 10^{19} cm^{-3}. The device initially demonstrates digital resistive switching behavior, characterized by an ON–OFF resistance ratio of $\sim 10^4$. Moreover, the device exhibits multilevel data storage capabilities, which can be controlled by adjusting the current compliance during the switching process. Further, the device exhibits analog resistive switching behavior with modulation of the switching parameters such as the applied voltage and voltage sweep rate. The temperature dependent switching studies indicate non-filamentary switching characteristics, which are attributed to the trapping and de-trapping of charge carriers at vacancy or trap sites, coupled with the migration of Cu^+-ions from the top copper electrode.

Introduction

Over the years, digital resistive switching memory, characterized by discrete and sharp SET/RESET processes, has been widely employed for data storage applications. However, as data storage demands continue to grow exponentially with requirements of faster switching speed, digital memory technologies are facing significant limitations due to the von Neumann bottleneck. As a result, there is growing interest in alternative memory paradigms, particularly for neuromorphic computing, where the continuous and gradual transition of resistance states during the SET/RESET processes, referred to as analog resistive switching, offers distinct advantages over digital switching. Analog switching provides more nuanced and energy-efficient control of memory states, making it a more suitable approach for mimicking biological neural processes.[1,2]

In this context, materials such as metal halides and sulfides including AgI, CuI, Ag_2S, and $Cu_{2-x}S$ (x ranges between 0 and 1) are emerging as promising candidates for

analog resistive switching due to their mixed ionic and electronic conductivities.[3,4] Among these, copper sulfide stands out for its properties such as high chemical stability, biocompatibility, non-toxicity, good optical absorption in the visible-NIR region, and thermal stability, making it attractive in various applications such as photocatalysis, solar cells, batteries, optical filters, switching and in biomedical applications.[5–10] Copper sulfide can exist in many stable and metastable states with varying stoichiometry, ranging from CuS to Cu_2S depending upon the Cu content. In the Cu_2S stoichiometry, it acts as an intrinsic semiconductor with a low carrier concentration (10^{15}–10^{16} cm^{-3}) due to a completely filled valence band.[11] However, in the Cu-deficient CuS, many Cu^{2+} vacancies are created, leading to an increased hole concentration ($\sim 10^{22}$ cm^{-3}).[12–14] This makes CuS more conductive and enables it to behave as a degenerate semiconductor.[15] Furthermore, as a solid electrolyte, CuS is highly accommodative of Cu^+-ions, facilitated by the redox state changes of the sulfide framework.[16] However, the reports on copper sulfide based resistive switching devices are scarce, particularly analog switching.[17] In a comparative study, Lim *et al.* observed threshold switching in Cu_2S and CuS-based cells with symmetric tungsten electrodes.[18] While Cu_2S demonstrated a

[a] Solid State Ionics Laboratory, Department of Physics, National Institute of Technology Silchar, Silchar-788010, Assam, India. E-mail: saumya@phy.nits.ac.in
[b] School of Physics, Sambalpur University, Jyoti Vihar, Burla, Odisha 768019, India

high off–on ratio and good non-linearity, the CuS device exhibited poor non-linearity and on–off ratio. Recently, there have been a few studies of copper sulfide-based memristors where the switching layer ($Cu_{2-x}S$) was deposited either *via* sulfurization or dry transfer method from its single crystal, which are cumbersome.[19,20]

In this work, we fabricated a memristive device based on copper sulfide, using copper (Cu) as the active electrode. A copper sulfide thin film was deposited using the chemical bath deposition (CBD) method, chosen for its simplicity, low cost, and ease of control over deposition parameters such as temperature, pH of the solution, deposition time, and precursor solution concentration.[10] The XPS and EDS investigation confirmed that the CBD-grown copper sulfide was neither purely in the form of Cu_2S nor CuS, rather, it formed polymorphic $Cu_{2-x}S$. The $Cu/Cu_{2-x}S$/ITO device exhibits digital resistive switching behavior, with an ON–OFF resistance ratio of ~10^4. As a precursor to analog switching, the device also demonstrates multibit data storage capability by varying the current compliance during the switching process. Subsequently, analog resistive switching behavior was also observed, with modulation of the switching characteristics achieved by adjusting the applied voltage and voltage sweep rate. The switching mechanism is attributed to the trapping and de-trapping of charge carriers at the trap/ vacancy sites, with contribution of Cu^+-ions migrating from the top Cu electrode.

Experimental

Preparation and fabrication of the copper sulfide-based memristor

The copper sulfide ($Cu_{2-x}S$) thin film was deposited onto an ITO/PET substrate *via* the chemical bath deposition (CBD) method.[21] For the preparation of copper sulfide using the CBD method, we sourced copper(ɪɪ) chloride dihydrate ($CuCl_2·2H_2O$), triethanolamine ($C_6H_{15}NO_3$), thiourea ($CS(NH_2)_2$) and ammonium solution (NH_4OH) from Merck. The ITO-coated PET (ITO/PET) substrate was purchased from Sigma-Aldrich. The ITO/PET substrate was cut into 1.8×1.8 cm^2. Initially, 1 M $CuCl_2·2H_2O$ and 1 M thiourea solutions were separately prepared in 3 ml and 10 ml of distilled (DI) water, respectively. Subsequently, 10 ml of triethanolamine (TEA) was added to the $CuCl_2·2H_2O$ solution and stirred for 30 minutes. Finally, 10 ml of the ammonia solution, 1 M thiourea solution, and 30 ml of DI water were added to the above solution and stirred for 2 h to obtain a homogeneous solution. The ITO/PET substrate was then vertically immersed in the solution, and the $Cu_{2-x}S$ film was deposited at 60 °C for 1 h. The film deposited onto the ITO/PET substrate was extracted from the solution, rinsed with DI water, and dried in a vacuum oven at 70 °C for 12 h. The thickness of the $Cu_{2-x}S$ film was estimated to be ~130 nm, as measured using an optical thickness meter. Following the drying process, a 40 nm circular Cu top electrode with a diameter of 100 µm

was deposited using the thermal evaporation method, employing a stainless-steel shadow mask. Consequently, a vertical two-terminal $Cu/Cu_{2-x}S$/ITO memristive device was fabricated, where Cu and ITO serve as the top and bottom electrodes, respectively.

Characterization of materials and devices

The structural and optical characterization of the copper sulfide thin film was carried out by using a PANalytical Xpert[3] powder X-ray diffractometer (XRD) with a Cu-$K\alpha_1$ source of wavelength 1.54 Å and an Agilent Cary 5000 UV-vis-NIR spectrophotometer, respectively. The microstructure and elemental analysis were carried out using SEM (JSM-IT200). The spectroscopic characterization of the copper sulfide film was conducted by using a Thermo Fisher Scientific K-alpha X-ray photoelectron spectrometer (XPS) with an Al K_α source. A Keithley 4200 semiconductor characterization system (SCS) was used for the electrical characterization of the copper sulfide-based memristive devices.

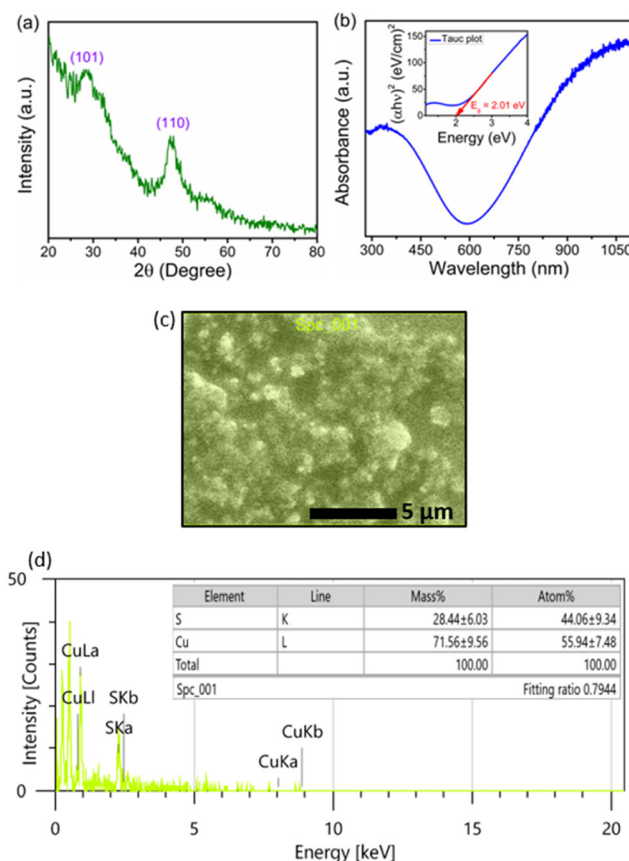**Fig. 1** (a) XRD pattern of the CBD copper sulfide film onto the ITO/ PET substrate. (b) UV-visible absorption spectra of CBD copper sulfide film. The inset of (b) shows the determination of the band gap energy from the Tauc plot. (c) SEM image and (d) EDS spectra of copper sulfide thin film.

© 2026 The Author(s). Published by the Royal Society of Chemistry

RSC Appl. Interfaces, 2026, **3**, 168–175 | 169

Results and discussion

Material characterization

The X-ray diffraction (XRD) pattern of the copper sulfide thin film deposited onto the ITO/PET substrate is presented in Fig. 1(a). The pattern exhibits two broad peaks at 28.5° and 48.2°, corresponding to the (101) and (110) planes that belong to covellite CuS (JCPDS card no. 06-0464).[22,23] However, as $Cu_{1.75}S$ and Cu_2S have Bragg peaks for the (101) and (110) planes near the same 2θ values, we cannot rule out the possibility of other phases along with covellite CuS.[24] The average crystallite size for the (101) and (110) peaks was determined to be 3.18 nm and 3.16 nm, respectively, using the Debye–Scherrer formula. Fig. 1(b) displays the UV-visible-NIR spectrum of the copper sulfide thin film across a wavelength range of 280–1100 nm. The spectrum reveals absorption in the near UV region (300–400 nm) and reaches a minimum around 590 nm. Notably, the absorption intensity does not drop to zero but rather increases significantly from 750 to 1100 nm in the NIR region. The rise in intensity is attributed to inter-band transitions from the valence states to the unoccupied states, which is characteristic of copper sulfide.[25,26] The band gap energy of the deposited film was estimated from the Tauc plot, as shown in the inset of Fig. 1(b). The band gap is ~2.01 eV, closely matching the reported value.[27] The variation in stoichiometry of copper in copper sulfide can significantly change the absorption spectrum. The observed absorption spectrum in this study matches more closely with that of $Cu_{1.75}S$, as reported by Zhu et al.[24] Hence, the deposited copper sulfide may not be in the pure covellite CuS phase, which is highly conducting in comparison to Cu-rich ($Cu_{2-x}S$, x varies between 0 and 1) phases. Hence, we assume that CBD copper sulfide has a polymorphic phase ($Cu_{2-x}S$).

The SEM image (Fig. 1(c)) reveals a uniform, void-free deposition of copper sulfide, though the surface microstructures exhibit a granular and non-uniform morphology. The EDS spectrum in Fig. 1(d) indicates a Cu:S atomic ratio of ~1.3:1, suggesting the formation of a copper-deficient polymorphic $Cu_{2-x}S$ phase.

To further confirm the oxidation states of copper in $Cu_{2-x}S$, we conducted X-ray photoelectron spectroscopy (XPS). The presence of C, O, Cu and S was confirmed from the XPS full scan survey as shown in Fig. 2(a). Then, the high-resolution spectra of C, O, Cu and S were separately investigated and are presented in Fig. 2(b)–(e). The high-resolution spectrum of C 1s (Fig. 2(b)) exhibits peaks at around 284.38, 285.94 and 288.06 eV due to C=C, C–OH and C=O,[24,28] which may be due to the surface absorbed hydrocarbons appearing from the reaction medium. In the high-resolution spectrum of O 1s as shown in Fig. 2(c), the peak observed at 532 eV is due to CO groups and confirms the absence of CuO (529.2 eV) or Cu_2O (530.2 eV) in the XPS spectra.[29] This O 1s spectrum is observed due to a reaction mechanism or adsorption from the environment. The high-resolution spectrum of Cu 2p is shown in
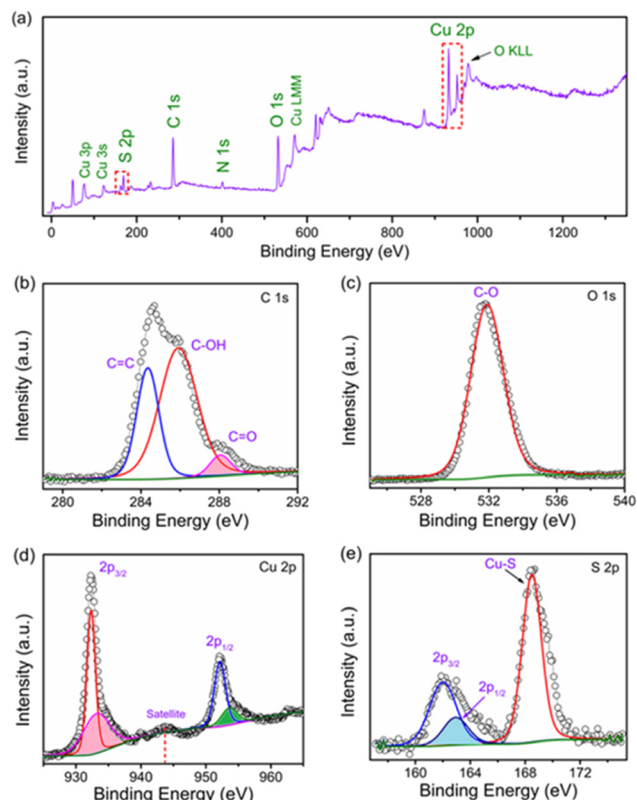

Fig. 2 (a) XPS full scan survey spectrum of the copper sulfide thin film. High resolution spectra of the (b) C 1s, (c) O 1s, (d) Cu 2p, and (e) S 2p regions.

Fig. 2(d). The two major peaks observed at 932 eV and 952 eV are assigned to $2p_{3/2}$ and $2p_{1/2}$, respectively, indicating the presence of the Cu^+ oxidation state. The two low-intensity deconvoluted peaks of $2p_{3/2}$ and $2p_{1/2}$ centered at 933.2 eV and 953.3 eV also reveal the presence of Cu^{2+} in the film. Further, a satellite peak of Cu^{2+} is observed at 943.6 eV in the Cu 2p spectrum.[24] This confirms that the CBD-grown copper sulfide has a mixed stoichiometry of copper with a greater Cu^+ fraction. In the precursor $CuCl_2 \cdot 2H_2O$, the oxidation state of copper is Cu^{2+}. However, the addition of thiourea as a sulfur source tends to convert Cu^{2+} to Cu^+.[30] In the high-resolution spectrum of S 2p, the peaks observed at 161.9 eV and 162.9 eV are assigned to S $2p_{3/2}$ and S $2p_{1/2}$ as shown in Fig. 2(e).[31] These two peaks arise due to the S^{2-} species. The additional peak at 168.5 eV is due to metal sulfides, i.e. Cu–S.[32] These studies confirm that the CBD-grown copper sulfide is polymorphic.

Memory characteristics of the $Cu/Cu_{2-x}S/ITO$ memristor

The current–voltage (I–V) characteristic of the $Cu/Cu_{2-x}S/ITO$ memristive device is presented in Fig. 3. A positive bias was applied to the copper top electrode and was swept cyclically from 0 to ±2 V as shown in Fig. 3(a). Initially, the device resides in the HRS. As the voltage sweeps from 0 to +2 V, the current gradually increases and undergoes an abrupt
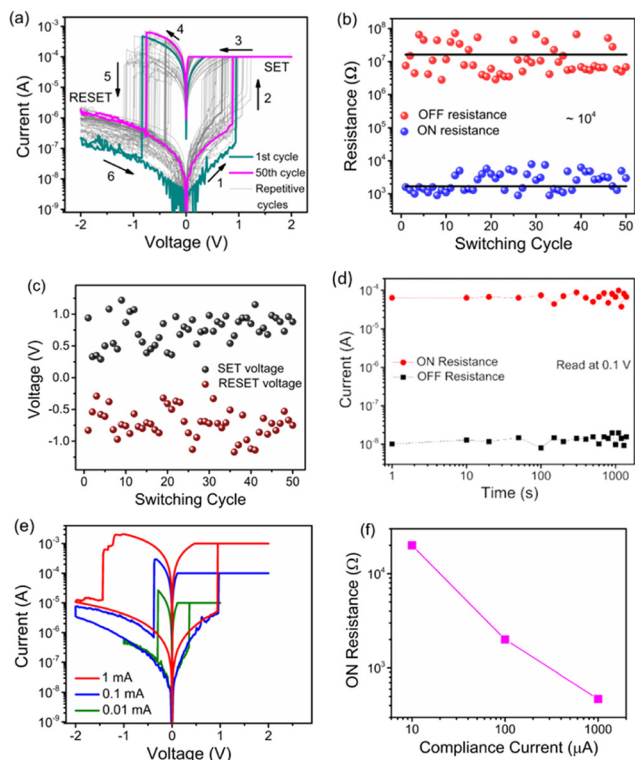
Fig. 3 (a) I–V characteristics of the Cu/Cu$_{2-x}$S/ITO memristive device showing bipolar digital RS behavior, (b) ON and OFF state resistances plotted as function of switching cycles, (c) plot of SET and RESET voltage with switching cycles, (d) retention test of the ON and OFF state, (e) multilevel I–V characteristics observed in the memristive device with varying compliance current, and (f) plot of ON state resistance (R_{ON}) with compliance current (CC).

Fig. 4 (a) I–V characteristics of the memristive device measured under four consecutive positive (1,2,3,4) and negative (5,6,7,8) voltage sweeps, (b) temporal evolution of four consecutive positive and negative voltage sweeps along with the current response, (c) plot of resistance ratio with consecutive positive and negative voltage sweeps, and (d) I–V plot of the memristive device in complete cycles by sweeping the voltage from 0 → 0.6 V → −0.6 V → 0.

transition to the LRS at a SET voltage of 0.94 V, persisting in the ON state. Conversely, during the voltage sweep from 0 to −2 V, the current experiences a sudden drop at a RESET voltage of −0.82 V. Therefore, bipolar digital non-volatile resistive switching is observed. The device operated without a forming process, as evidenced by the SET voltages of successive cycles remaining within the range of the initial cycle. The resistance ratio between the ON and OFF states is approximately 10^4. The variation in ON and OFF state resistances over 50 consecutive cycles is presented in Fig. 3(b). The cycle-to-cycle variation of both SET and RESET voltages lies between ±0.30 and ±1.20 V, as shown in Fig. 3(c). The mean SET voltage ($\mu \pm \sigma$) is (0.74 ± 0.24 V), while the mean RESET voltage is (−0.72 ± 0.23 V). The device also demonstrates stable retention for up to 1000 s under a read voltage of 0.1 V, as shown in Fig. 3(d). Fig. 3(e) displays the multilevel I–V characteristics obtained at compliance currents of 0.01, 0.1, and 1 mA. The ON-state resistance (R_{ON}) decreases systematically with increasing compliance current, as presented in the Fig. 3(f), with the corresponding values of 20 kΩ, 1.9 kΩ, and 470 Ω for 0.01, 0.1, and 1 mA, respectively.

Further, we tried observing analog switching by reducing the operational voltage range and maneuvering the voltage
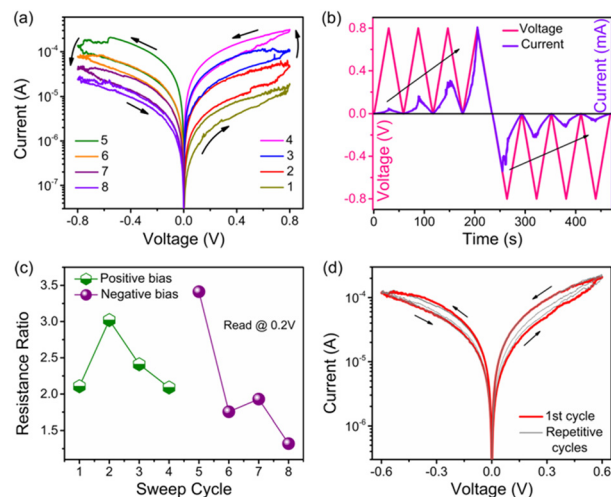
sweep rate. We successively biased the device in the positive direction with a sweeping sequence of 0 → 0.8 V → 0 for 4 consecutive sweeps, as delineated in Fig. 4(a). The device attained a new LRS as the voltage sweep progresses from the first to the 4th cycle. Conversely, upon applying bias voltage in the negative direction for 4 consecutive sweeps from 0 → −0.8 V → 0, the device's high resistance state (HRS) exhibited a gradual increase in resistance values as the voltage sweep progresses from the 5th to the 8th cycle. Typically, as the number of sweeping cycles increases on either the SET or the RESET side of the bias, the switching window sequentially decreases.[3] This occurs because new conductance states are established after each sweep, reducing the number of available states. However, in this Cu$_{2-x}$S-based memristor, the switching window of 2 observed during the first cycle is retained even after the fourth cycle, suggesting that multiple conductance states still remain accessible after the 4th cycle of sweeping in the positive bias direction. Fig. 4(a) is reproduced in Fig. 4(b) to show the temporal evolution of voltage sweeps and the corresponding current responses, analogically representing the potentiation and depression of synaptic weights under spiking activity. This behaviour highlights the incremental increase in conductance with successive positive sweeps, followed by a gradual decrease under consecutive negative sweeps. Moreover, the resistance ratio between the HRS and LRS during analog switching, read at 0.2 V, decreases as the number of voltage sweeps increases in both bias directions (Fig. 4(c)). The device was then biased across both polarities with a sweep sequence of 0 → 0.6 V → −0.6 V → 0, and the resulting I–V characteristics are shown in Fig. 4(d). As the voltage increases from 0 to +0.6 V, the current gradually rises, reaching the LRS, while a reverse

© 2026 The Author(s). Published by the Royal Society of Chemistry

RSC Appl. Interfaces, 2026, **3**, 168–175 | 171

sweep from 0 to −0.6 V restores the HRS. These results confirm that the Cu$_{2-x}$S-based memristor exhibits stable, repeatable analog switching behaviour. The hysteresis loops for positive and negative sweeps are nearly symmetrical, with switching windows of 1.92 and 1.53, respectively.

Switching mechanism

To investigate the current conduction mechanism of the Cu/Cu$_{2-x}$S/ITO memristive device, the I–V characteristics during the SET and RESET processes in the digital resistive switching mode were analyzed and plotted in a log–log scale, as depicted in Fig. 5(a) and (b). In the HRS, when the voltage was swept from 0 to the positive direction, the device displayed a linear relationship in the low voltage region from 0.03 to 0.17 V with a slope of 1.06. This behavior indicates ohmic conduction,[33] as shown in Fig. 5(a). As the voltage was increased further to the high voltage region (0.18 to 0.68 V), the I–V curve was fitted linearly with a slope of 2.21, suggesting that the conduction mechanism transitioned to trap-assisted space charge limited conduction (SCLC) with $I \propto V^m$, where $m > 2$.[1,34] In the LRS, the current conduction again follows ohmic conduction with a slope of 0.97. During the subsequent sweep in the negative bias direction, the current conduction continued to exhibit ohmic behavior, with a slope of 1.04 as shown in Fig. 5(b). After the RESET occurred at 0.80 V, the I–V curve was fitted linearly with a slope of 1.95 in the HRS, reflecting the detrapping of charge carriers from trap sites. As the voltage decreased further from 0.54 to 0.01 V, the current conduction followed ohmic behavior.

Further, to investigate the current conduction mechanism of analog switching, the I–V curve for the first positive voltage sweep (Fig. 4(a)) is plotted in the log–log scale, as shown in Fig. 5(c). It is observed that in the low biasing region, i.e., 0 < V < 0.6 V, the curve is fitted linearly with a slope of 1.02, indicating ohmic conduction. As the voltage increases further from 0.6 V < V < 0.8 V, the slope of the linearly fitted curve is 4.84. This suggests that the current conduction in the higher voltage region is dominated by the trap-assisted space-charge-limited conduction (SCLC). Thus, in the HRS, the current conduction is ohmic initially and then followed by trap assisted-SCLC. In the LRS, when sweeping back to zero from 0.8 V, the current conduction is again ohmic type in the entire biasing region, with a slope of 0.98. During the negative sweep direction, the current conduction is ohmic in the LRS with a slope of 1.01 for the entire biasing region. By returning the voltage sweep from −0.8 V to 0 V, in the voltage region −0.8 V to −0.7 V, the slope is found to be 4.43, indicating the detrapping of charge carriers (holes). Further, decreasing the voltage from −0.7 V to 0 V, the current conduction is ohmic with a slope of 1.04. Although the current conduction mechanism in both analog and digital switching is primarily governed by charge trapping and detrapping, these processes alone cannot account for the observed behaviour. Since copper is an active electrode, Cu$^+$ ions are also anticipated to participate in the switching dynamics. Devices employing inert electrodes with Cu$_2$S or CuS switching layers (e.g., W/Cu$_2$S or CuS/W) exhibited only diffusive volatile switching.[18] In contrast, our devices with Cu as the active electrode show non-volatile bipolar switching, indicating that Cu$^+$ ion injection from the top electrode plays a crucial role. Furthermore, trapping and detrapping of electrons or holes at defect sites complement, rather than exclude, the ionic contribution, as reported for TbMnO$_3$.[35] The involvement of intrinsic ion conduction has been highlighted in recent studies on Cu$_{2-x}$S and Cu$_2$S-based memristors, where switching was non-filamentary. In Cu$_{2-x}$S cells, Lee et al. reported Cu$^+$ ion depletion under bias leading to Cu-deficient CuS phase formation in the ON state, which reverts to Cu$_{2-x}$S upon bias reversal.[19] Qin et al. observed that Cu$^+$ ion migration induces a structural transition from monoclinic Cu$_2$S to tetragonal Cu$_{2-x}$S.[20]

To further verify the conduction mechanism, temperature-dependent I–V measurements were performed from 25 to 65 °C in 10 °C increments (Fig. 6(a)). With increasing temperature, both conductivity and SET voltage rise. Fig. 6(b) shows that ON resistance decreases with temperature, deviating from the metallic behaviour typical of filamentary switching in ECM cells.[35] These results suggest that the switching mechanism arises from charge carrier trapping/detrapping coupled with Cu$^+$-ion diffusion from the top electrode. The carrier concentration was estimated using the Mott–Schottky relation[36]

$$\frac{1}{C^2} = \frac{2}{\varepsilon \varepsilon_0 A^2 e N_A} \left(V - V_{fb} - \frac{k_B T}{e} \right) \qquad (1)$$

where, C is the interfacial capacitance, A is the area, N_A is the number of acceptors, V is the applied voltage, k_B is the Boltzmann constant, T is the absolute temperature, V_{fb} is the
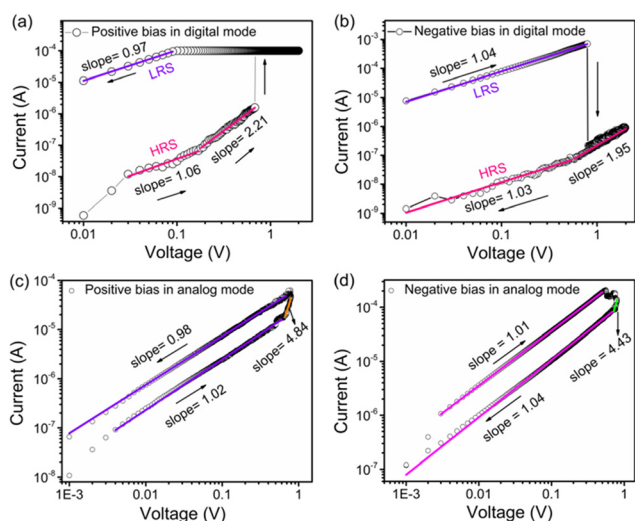

Fig. 5 log–log plots of a digital I–V curve for the (a) SET process and (b) RESET process in theCu/Cu$_{2-x}$S/ITO memristive device. log–log plots of an analog I–V for the first (c) positive and (d) negative voltage sweep of the device.
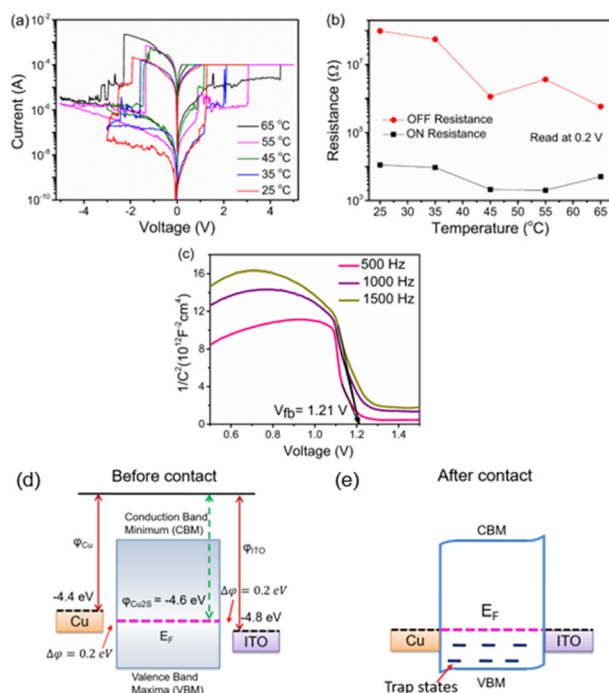
Fig. 6 (a) I–V characteristics of the first sweep cycle with temperature ranging from 25 to 65 °C, (b) ON and OFF resistance plots with temperature, and (c) Mott–Schottky plots of $Cu_{2-x}S$. Schematic of the energy band diagram of the $Cu/Cu_{2-x}S/ITO$ memristive device (d) before and (e) after contact.

flat band potential, ε_0 is the vacuum permittivity, ε is the dielectric constant of the $Cu_{2-x}S$ layer and e is the charge of electron. A plot of $1/C^2$ versus V is shown below in Fig. 6(c) at three different frequencies. The flat-band potential V_{fb} was determined by extrapolating the linear region of the plot to the voltage axis. Using the slope of this linear region, the value of carrier concentration N_A was calculated to be $\sim 10^{19}$ cm^{-3}. To understand the current conduction mechanism, the band diagram of the memristive device is shown in Fig. 6(d) and (e). The work function of $Cu_{2-x}S$ is $\varphi \approx -4.6$ eV,[32] which closely matches with the work function of Cu ($\varphi \approx -4.4$ eV) and ITO ($\varphi \approx -4.8$ eV).[37–40] Consequently, both interfaces—$ITO/Cu_{2-x}S$ and $Cu/Cu_{2-x}S$—exhibit ohmic rather than Schottky behaviour. Thus, the rectification effect typically observed at Schottky contacts is absent in this case.[3] The polymorphic $Cu_{2-x}S$-based device therefore behaves as an ohmic memristor, offering symmetric potentiation and depression characteristics, albeit with a reduced switching window due to the lack of Schottky barriers.[41] Further improvements can be achieved by optimizing parameters such as the Cu-to-S stoichiometric ratio, the thickness of the $Cu_{2-x}S$ switching layer, and the choice of electrode materials.

Conclusions

In summary, a copper sulfide-based memristive device was fabricated using the chemical bath deposition (CBD) method, with copper (Cu) serving as the active electrode. Polymorphic $Cu_{2-x}S$ is confirmed by EDS and XPS. The memristor exhibits digital resistive switching behavior, characterized by variation in the SET and RESET voltages, with an ON–OFF resistance ratio of $\sim 10^4$. Furthermore, the device demonstrates multilevel data storage capability, which can be controlled by adjusting the current compliance during the switching process. Notably, analog resistive switching behavior was also observed in the copper sulfide-based device, with modulation of the switching characteristics achievable by varying parameters such as the applied voltage and voltage sweep rate. The underlying switching mechanism is attributed to the trapping and de-trapping of charge carriers at vacancy or trap sites, with the migration of Cu^+-ions from the top copper electrode. The observation of simultaneous digital and analog switching in $Cu_{2-x}S$ memristive devices can be further explored for neuromorphic application.

Author contributions

All the authors contribute equally.

Conflicts of interest

There are no conflicts of interest to declare.

Data availability

The raw data supporting the findings of this study were generated at the National Institute of Technology Silchar. These data are available from the corresponding author, S. R. M., upon reasonable request.

Acknowledgements

References

1 R. Deb, M. G. Nair, U. Das and S. R. Mohapatra, Contrasting analog and digital resistive switching memory characteristics in solution-processed copper(I) thiocyanate and its polymer electrolyte-based memristive devices, *J. Mater. Chem. C*, 2023, **11**, 7629–7640.

2 A. Sebastian, M. L. Gallo, R. K. Aljameh and E. Eleftheriou, Memory devices and applications for in-memory computing, *Nat. Nanotechnol.*, 2020, **15**, 529–544.

3 R. Deb, S. Mallik, Y. Mishra, R. Padhan, S. Sahoo, K. Terabe, T. Tsuruoka and S. R. Mohapatra, Bias Sweep-Induced Analog Memristor Behavior, Using a Cuprous Iodide Thin Film, for Neuromorphic Computing, *ACS Appl. Electron. Mater.*, 2025, **7**, 4616–4627.

4 Y. Zhu, T. Nyberg, L. Nyholm, D. Primetzhofer, X. Shi and Z. Zhang, Wafer-Scale Ag2S-Based Memristive Crossbar Arrays with Ultra-Low Switching-Energies Reaching Biological Synapses, *Nano-Micro Lett.*, 2024, **17**, 69.

© 2026 The Author(s). Published by the Royal Society of Chemistry

RSC Appl. Interfaces, 2026, **3**, 168–175 | 173

5   G. Nabia, M. Tanveera, M. B. Tahira, M. Kirana, M. Rafiquec, N. R. Khalida, M. Alzaidd, N. Fatimaa and T. Nawaz, Mixed solvent based surface modification of CuS nanostructures for an excellent photocatalytic application, *Inorg. Chem. Commun.*, 2020, **121**, 108205.

6   H. Lei, G. Fang, F. Cheng, W. Ke, P. Qin, Z. Song, Q. Zheng, X. Fan, H. Huang and X. Zhao, Enhanced efficiency in organic solar cells via in situ fabricated p-type copper sulfide as the hole transporting layer, *Sol. Energy Mater. Sol. Cells*, 2014, **128**, 77–84.

7   D. Ayodhya and G. Veerabhadram, Investigation of temperature and frequency dependence of electrical conductivity and dielectric behavior in CuS and rGO capped CuS nanocomposites, *Mater. Res. Express*, 2019, **6**, 045910.

8   L. Chen, W. Yu and Y. Li, Synthesis and characterization of tubular CuS with flower-like wall from a low temperature hydrothermal route, *Powder Technol.*, 2009, **191**, 52–54.

9   L. Wang, Synthetic methods of CuS nanoparticles and their applications for imaging and cancer therapy, *RSC Adv.*, 2016, **6**, 82596–82615.

10 B. B. Chaudhari, N. P. Huse, N. P. Huse and R. B. Sharma, In-situ Facile Chemical Bath Deposition of CuS Thin Film for Photosensor Application, *Journal of Applied Science and Computations*, 2019, **VI**, 2175–2180.

11 S. C. Riha, R. D. Schaller, D. J. Gosztola, G. P. Wiederrecht and A. B. F. Martinson, Photoexcited Carrier Dynamics of Cu₂S Thin Films, *J. Phys. Chem. Lett.*, 2014, **5**(22), 4055–4061.

12 D. Ayodhya and G. Veerabhadram, A review on recent advances in photodegradation of dyes using doped and heterojunction based semiconductor metal sulfide nanostructures for environmental protection, *Mater. Today Energy*, 2018, **9**, 83–113.

13 A. T. Sheardy, D. M. Arvapalli and J. Wei, Novel microwave synthesis of near-metallic copper sulfide nanodiscs with size control: experimental and DFT studies of charge carrier density, *Nanoscale Adv.*, 2020, **2**, 1054–1058.

14 R. Deb, D. Panda, M. G. Nair, F. Yasmin, Y. Mishra, A. K. Thakur and S. R. Mohapatra, Diffusive Memristor with CuS Nanoparticles Embedded in Polymeric Film as Artificial Nociceptor, *ACS Appl. Mater. Interfaces*, 2024, **16**, 51757–51768.

15 S. S. Kalanura and H. Seo, Tuning plasmonic properties of CuS thin films via valence band filling, *RSC Adv.*, 2017, **7**, 11118–11122.

16 Y. Xie, A. Riedinger, M. Prato, A. Casu, A. Genovese, P. Guardia, S. Sottini, C. Sangregorio, K. Miszta, S. Ghosh, T. Pellegrino and L. Manna, Copper Sulfide Nanocrystals with Tunable Composition by Reduction of Covellite Nanocrystals with Cu⁺ Ions, *J. Am. Chem. Soc.*, 2013, **135**(46), 17630–17637.

17 A. Nayak, T. Ohno, T. Tsuruoka, K. Terabe, T. Hasegawa, J. K. Gimzewski and M. Aono, Controlling the Synaptic Plasticity of a Cu₂S Gap-Type Atomic Switch, *Adv. Funct. Mater.*, 2012, **22**, 3606–3613.

18 S. Lim, J. Yoo, J. Song, J. Woo, J. Park and H. Hwang, CMOS compatible low-power volatile atomic switch for steep-slope FET devices, *Appl. Phys. Lett.*, 2018, **113**, 033501.

19 S. Lee, J. Byeon, S. Park, T. Kim, J. Lim, J. Kim, E. Cho, J. Lee, S. Pak and S. N. Cha, Non-volatile resistive switching characteristics in Cu₂₋ₓS-based memristor, *Nanoscale*, 2025, **17**, 21217–21223.

20 L. Qin, Y. Yu, C. Fang, Y. Liu, K. Zhu, D. Ouyang, S. Liu, B. Song, R. Zhou, M. Lanza, W. Hu, J. Wu, Y. Li and T. Zhai, Intrinsic ion migration-induced susceptible two-dimensional phase- transition memristor with ultralow power consumption, *Sci. Bull.*, 2025, **70**, 2116–2124.

21 S. U. Offiah, P. E. Ugwoke, A. B. C. Ekwealor, S. C. Ezugwu, R. U. Osuji and F. I. Ezema, Structural and spectral analysis of chemical bath deposited copper sulfide thin films for solar energy conversions, *Dig. J. Nanomater. Biostruct.*, 2012, **7**, 165–173.

22 Y. L. Auyoong, P. L. Yap, X. Huang and S. B. A. Hamid, Optimization of reaction parameters in hydrothermal synthesis: a strategy towards the formation of CuS hexagonal plates, *Chem. Cent. J.*, 2013, **7**, 1–12.

23 J. Li, T. Jiu, G. H. Tao, G. Wang, C. Sun, P. Li, J. Fang and L. He, Manipulating surface ligands of Copper Sulfide nanocrystals: Synthesis, characterization, and application to organic solar cells, *J. Colloid Interface Sci.*, 2014, **419**, 142–147.

24 Y. Zhu, Y. Lu, S. H. Sun, B. Zhou and Y. M. Hu, Phase Selectivity of Copper Sulfide: Synthesis and Application, *J. Electron. Mater.*, 2021, **50**, 2034–2042.

25 M. Tanveer, C. Cao, Z. Ali, I. Aslam, F. Idrees, W. S. Khan, F. K. But, M. Tahir and N. Mahmood, Template free synthesis of CuS nanosheet-based hierarchical microspheres: an efficient natural light driven photocatalyst, *CrystEngComm*, 2014, **16**, 5290–5300.

26 W. Zhong, N. Yu, L. Zhang, Z. Liu, Z. Wang, J. Hu and Z. Chen, Synthesis of CuS nanoplate-containing PDMS film with excellent near-infrared shielding properties, *RSC Adv.*, 2016, **6**, 18881–18890.

27 D. Ayodhya and G. Veerabhadram, A review on recent advances in photodegradation of dyes using doped and heterojunction based semiconductor metal sulfide nanostructures for environmental protection, *Mater. Today Energy*, 2018, **9**, 83–113.

28 G. Y. Shaikh, D. S. Nilegave, S. S. Girawale, K. B. Kore, S. R. Newaskar, S. A. Sahu and A. M. Funde, Structural, Optical, Photoelectrochemical, and Electronic Properties of the Photocathode CuS and the Efficient CuS/CdS Heterojunction, *ACS Omega*, 2022, **7**, 30233–30240.

29 M. Das, D. Das, S. Sil and P. P. Ray, Development of hierarchical copper sulfide– carbon nanotube (CuS–CNT) composites and utilization of their superior carrier mobility in efficient charge transport towards photodegradation of Rhodamine B under visible light, *Nanoscale Adv.*, 2023, **5**, 3655–3663.

30 A. Rahmani, H. Rahmani and A. Zonouzi, Synthesis of copper sulfides with different morphologies in DMF and

water: catalytic activity for methyl orange reduction, *Mater. Res. Express*, 2017, **4**, 125024.

31 Tarachand, S. Hussain, N. P. Lalla, Y. K. Kuo, A. Lakhani, V. G. Sathe, U. Deshpande and G. S. Okram, Thermoelectric properties of Ag-doped CuS nanocomposites synthesized by a facile polyol method, *Phys. Chem. Chem. Phys.*, 2018, **20**, 5926–5935.

32 D. Tahir and S. Tougaard, Electronic and optical properties of Cu, CuO and Cu_2O studied by electron spectroscopy, *J. Phys.: Condens. Matter*, 2012, **24**, 175002.

33 R. Deb, P. Pathak, S. R. Mohapatra and U. Das, Polarity independent resistive switching in MoS_2 nanosheets and PEO-based nanocomposite films, *Jpn. J. Appl. Phys.*, 2022, **61**, SM1004.

34 Y. Li, J. Chu, W. Duan, G. Cai, X. Fan, X. Wang, G. Wang and Y. Pei, Analog and Digital Bipolar Resistive Switching in Solution Combustion-Processed NiO Memristor, *ACS Appl. Mater. Interfaces*, 2018, **10**, 24598–24606.

35 Y. Cui, H. Peng, S. Wu, R. Wang and T. Wu, Complementary Charge Trapping and Ionic Migration in Resistive Switching of Rare-Earth Manganite TbMnO3, *ACS Appl. Mater. Interfaces*, 2013, **5**, 1213–1217.

36 K. Gelderman, L. Lee and S. W. Donne, Flat-Band Potential of a Semiconductor: Using the Mott–Schottky Equation, *J. Chem. Educ.*, 2007, **84**, 685.

37 Z. H. Li, K. O. Egbo, X. H. Lv, Y. Wang, K. M. Yu and C. P. Liu, Electronic structure and properties of $Cu_{2-x}S$ thin films: Dependence of phase structures and free-hole concentrations, *Appl. Surf. Sci.*, 2022, **572**, 151530.

38 G. Giovannetti, P. A. Khomyakov, G. Brocks, V. M. Karpan, J. V. D. Brink and P. J. Kelly, Doping Graphene with Metal Contacts, *Phys. Rev. Lett.*, 2008, **101**, 026803.

39 C. T. Tsai, S. R. Gottam, P. C. Kao, D. C. Perng and S. Y. Chu, Improvement of OLED performances by applying annealing and surface treatment on electro-deposited CuSCN hole injection layer, *Synth. Met.*, 2020, **269**, 116537.

40 J. Rittich, S. Jung, J. Siekmann and M. Wuttig, Indium-Tin-Oxide (ITO) Work Function Tailoring by Covalently Bound Carboxylic Acid Self-Assembled Monolayers, *Phys. Status Solidi B*, 2018, **255**, 1800075.

41 S. Chen, Z. Yang, H. Hartmann, A. Besmehn, Y. Yang and I. Valov, Electrochemical ohmic memristors for continual learning, *Nat. Commun.*, 2025, **16**(1), 2348.